



Extended Ganglion Cell Layer Thickness Deviation Maps With OCT in Glaucoma Diagnosis

Paul Lehmann[†], Bettina Hohberger[†], Robert Lämmer and Christian Mardin^{*}

Department of Ophthalmology, University of Erlangen-Nürnberg, Friedrich-Alexander-University of Erlangen-Nürnberg, Erlangen, Germany

OPEN ACCESS

Edited by:

Michele Lanza,
University of Campania Luigi
Vanvitelli, Italy

Reviewed by:

Brent Siesky,
Icahn School of Medicine at Mount
Sinai, United States
Christoph Faschinger,
Private Practitioner, Graz, Austria
Huiyuan Hou,
University of California, San Diego,
United States
Feng Wen,
Sun Yat-sen University, China

*Correspondence:

Christian Mardin
christian.mardin@uk-erlangen.de

[†]These authors have contributed
equally to this work and share
first authorship

Specialty section:

This article was submitted to
Ophthalmology,
a section of the journal
Frontiers in Medicine

Received: 23 March 2021

Accepted: 30 April 2021

Published: 04 June 2021

Citation:

Lehmann P, Hohberger B, Lämmer R
and Mardin C (2021) Extended
Ganglion Cell Layer Thickness
Deviation Maps With OCT in
Glaucoma Diagnosis.
Front. Med. 8:684676.
doi: 10.3389/fmed.2021.684676

Purpose: The aim of the present study was to investigate the diagnostic power of RGCL in the macula quantitatively and qualitatively by using a conventional and extended elliptic grid with deviation maps.

Subjects and Methods: Thickness of RGCL was measured using SPECTRALIS[®] OCT (Heidelberg Engineering, Heidelberg, Germany) in 150 eyes of 150 subjects of the Erlangen Glaucoma Registry (EGR; NTC00494923): 26 ocular hypertension (OHT), 39 pre-perimetric open-angle glaucoma (pre-OAG), 19 normal tension glaucoma (NTG), 34 primary open-angle glaucoma (POAG), 16 secondary open-angle glaucoma (SOAG), and 16 controls. Analysis of RGCL was done quantitatively (global value, GV) and qualitatively (qualitative total value, QTV) by using a color-coded point score for data of the common elliptic macular grid of deviation maps. Furthermore, qualitative analysis of RGCL was done for an extended elliptic macula grid (extended qualitative total value, eQTV). Receiver operating characteristic (ROC) curves were calculated for the conventional and the enlarged macular grid for all subjects' groups.

Results: GV of RGCL thickness differed significantly between pre-OAG ($p < 0.05$), NTG ($p < 0.001$), POAG ($p < 0.001$), SOAG ($p < 0.001$), yet not OHT ($p > 0.05$) and controls, respectively. Quantitative ROC analysis of GV showed AUC of 0.965 (SOAG), 0.942 (POAG), 0.916 (NTG), 0.772 (pre-OAG), and 0.526 (OHT). QTV differed significantly between pre-POAG ($p < 0.05$), NTG ($p < 0.001$), POAG ($p < 0.001$), SOAG ($p < 0.001$), yet not OHT ($p > 0.05$) and controls, respectively. Qualitative ROC analysis of QTV showed AUCs of 0.908 (NTG) 0.914 (POAG), 0.930 (SOAG), 0.734 (pre-POAG), and 0.519 (OHT). Implementation of eQTV yielded even higher AUCs for NTG (0.919), POAG (0.969), and SOAG (0.973) compared to GV. Similar AUCs of eQTV and GV were observed for OHT (0.514) and pre-OAG (0.770).

Conclusion: The results of the present study showed that quantitative and qualitative analysis of RGCL thickness yielded similar diagnostic impacts compared to RNFL. Qualitative analysis might be a quick and easy useable tool for clinical all-day life. The present data suggest that analysis of an extended macula region might improve its diagnostic impact.

Keywords: retinal ganlion cell, OCT, spectralis, glaucoma, GRID

INTRODUCTION

Glaucoma is one of the most common causes of blindness worldwide. The health burden caused by glaucoma increased in the last 25 years (1, 2). Several risk factors are involved in the multifactorial pathogenesis of this neurodegenerative disease (3) including advanced age, positive family history, severe myopia, and its main risk factor an elevated intraocular pressure (IOP) (4, 5). It is assumed that high IOP triggers retinal ganglion cell (RGC) loss (6). Loss of RGCs occurs before functional abnormalities can be seen in a patient's perimetry (7).

Optical coherence tomography (OCT) offers the ability to examine characteristics of the retina and optic nerve head of glaucoma patients in an objective and non-invasive way (8). Thereby, scan quality reaches to the level of histological images. It seems to be more precisely than perimetry for diagnosing the progression of glaucoma in earlier stages (9). Next to measurement of the peripapillary retinal nerve fiber layer (RNFL), RGC layer (RGCL) thickness can be quantified (10). The RNFL thinning decreases in speed while glaucoma disease continues to progress. In contrast, RGCL thickness continued to decrease constantly with glaucoma progression (9). Thus, analysis of RGCL thickness might offer an additional diagnostic parameter for revealing progression of glaucoma from early to advanced stages. In eyes with early pre-perimetric glaucoma average RGCL thickness and especially the inferior region of the macula RGCL were observed to be the most appropriate ones for diagnostics (7). Implementation of enlarged grids for RGCL analysis, enabling analysis of larger macula regions, lead to an enhanced diagnostic power, as temporal quadrants of larger macular grids reached highest AUC value (11).

Most of the recent studies analyzed the ganglion cell complex (GCC), consisting of the inner plexiform layer (IPL), ganglion cell layer (GCL), and retinal nerve fiber layer (RNFL) (12) or GCIPL (i.e., GCL and IPL) (13, 14). To best of our knowledge, we did not find a study in literature focusing on single RGCL thickness in patients with different types of glaucoma. However, a finer analysis of macular retinal layers could identify distinct alterations of retinal ganglion cells. Thus, by analyzing single RGCL thickness, very fine changes in RGCL could be detected at even earlier stages of disease. The aim of the present study was to investigate the diagnostic power of only RGCL in the macula quantitatively and qualitatively by using a conventional and extended elliptic grid in patients with ocular hypertension (OHT), pre-perimetric open-angle glaucoma (pre-OAG), normal tension glaucoma (NTG), primary open-angle glaucoma (POAG), and secondary open-angle glaucoma (SOAG) compared to controls. In addition, RGCL data were compared to RNFL in patients' groups.

MATERIALS AND METHODS

Patients

One hundred fifty eyes of 150 patients of the Erlangen Glaucoma Registry (EGR; NTC00494923) of the Department of Ophthalmology of the University of Erlangen-Nürnberg were

TABLE 1 | Classification of perimetric glaucoma patients (NTG, POAG, SOAG) into subgroups based on mean defect (MD, Octopus perimetry): mild, moderate, and advanced; ratio represents percentage of disease severity in all perimetric glaucoma eyes.

Severity	Total ratio %	NTG	POAG	SOAG
Mild MD \leq 6 dB	30.4	5	11	5
Moderate MD > 6 dB and \leq 12 dB	33.3	10	9	4
Advanced MD > 12 dB	36.2	4	14	7

analyzed retrospectively: 26 ocular hypertension (OHT), 39 pre-perimetric open-angle glaucoma (pre-OAG), 19 normal tension glaucoma (NTG), 34 primary open-angle glaucoma (POAG), 16 secondary open-angle glaucoma (SOAG), and 16 controls. The EGR is a longitudinal follow-up study under therapy, including subjects with manifest glaucoma, glaucoma suspects, and a control group. All patients received an ophthalmic examination, including slit lamp microscopy, funduscopy, and gonioscopy. IOP was measured by Goldmann applanation tonometry. Visual field was tested using white-on-white Octopus perimetry (mean defect, MD; Octopus 500, 900; program G1, Interzeag, Schlieren, Schweiz, Peridata Software). Demographic data of all subjects can be seen in **Table 1**.

Diagnosis was done according to the following criteria:

OHT

Diagnosis of OHT was based on an increased IOP > 21 mmHg (repeated twice). Optic nerve head and visual fields showed no pathological alterations.

Pre-OAG

Pre-OAG showed an increased IOP > 21 mmHg (repeated twice), alterations of the optic nerve head, classified according to Jonas et al. (15) Visual field was normal.

POAG

Diagnosis of POAG was based on an increased IOP > 21 mmHg (repeated twice), alterations of the optic nerve head, classified according to Jonas et al. Visual field defects were detected according to the following criteria: Scotomas with \geq 3 neighboring test points on the pattern deviation map with a probability of <5%, \geq 2 adjacent test points on the pattern deviation map with a probability of <1% and MD > 2.8 dB. These perimetric defects had to be located at the same side in at least 2 consecutive examinations.

NTG

Diagnosis of NTG was as for POAG (see above), yet IOP was within normal ranges \leq 21 mmHg.

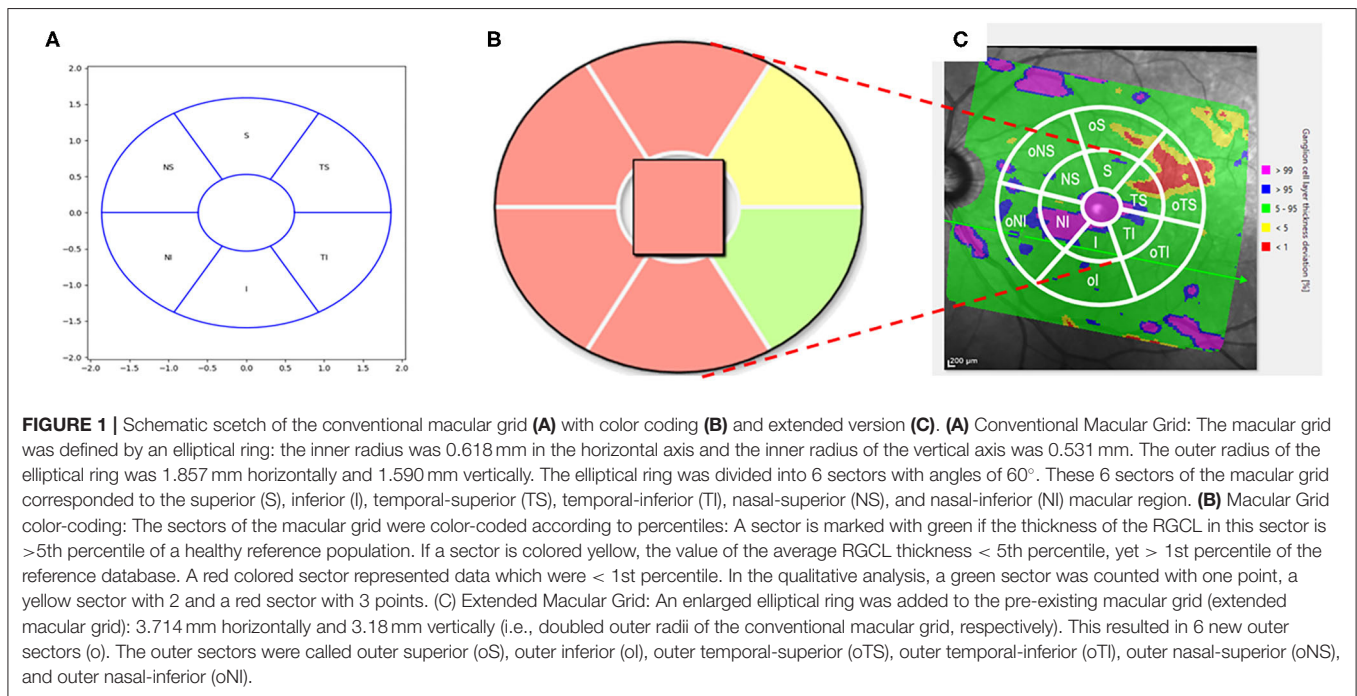
SOAG

Patients meeting criteria of POAG and additionally were affected by pseudoexfoliation syndrome (7) or melanin dispersion (9) were classified as SOAG.

If both eyes met the inclusion criteria, one eye of each person was selected randomly for the present analysis. Glaucoma

TABLE 2 | Demographic data: median and quartiles [of all subgroups (OHT, pre-OAG, POAG, NTG, SOAG, controls); Gender [m/f], Age [years], BCVA, IOP [mmHg], MD [dB], and RNFL [μm].

	Gender [m/f]	Age [years]	BCVA	IOP [mmHg]	MD [dB]	Global RNFL [μm]
OHT	13/13	60.0 (49.8–71.3)	0.8 (0.8–1.0)	17.0 (15.0–19.0)	2.18 (0.9–3.4)	94.0 (88.0–103.3)
Pre-OAG	20/19	66.0 (60.0–75.0)	1.0 (0.8–1.0)	14.0 (12.0–17.0)	2.5 (1.1–4.4)	76.0 (64.0–84.0)
NTG	6/13	75.0 (66.0–80.0)	0.7 (0.5–0.9)	10.0 (10.0–13.0)	9.1 (4.5–12.0)	62.0 (55.0–73.0)
POAG	15/19	71.0 (65.5–78.0)	0.8 (0.6–0.9)	13.0 (11.8–15.0)	9.65 (4.4–13.9)	55.5 (48.0–72.8)
SOAG	10/6	66.0 (56.0–75.3)	0.63 (0.5–1.0)	12.5 (10.0–14.8)	9.7 (5.1–17.1)	59.0 (49.3–67.3)
Controls	5/11	57.5 (51.3–66.5)	0.95 (0.8–1.0)	13.5 (12.0–16.0)	1.33 (0.2–2.7)	90.0 (87.0–96.0)



patients were classified into 3 groups based on the severity of visual field defect in Octopus perimetry. Mild glaucoma was defined as MD ≤ 6 dB. Moderate glaucoma was present when the patient's MD was >6 dB and ≤ 12 dB. Advanced glaucoma was allocated when MD was >12 dB. Classification of patients with mild, moderate and advanced glaucoma can be seen in **Table 2**.

Controls

Control eyes showed an IOP within normal ranges ≤ 21 mmHg, no alterations of the optic nerve head and a normal visual field. MD was ≤ 2.8 dB. Less than 3 adjacent test points on the pattern deviation map with a probability of $<5\%$ and <2 adjacent test points on the pattern deviation map with a probability of $<1\%$.

Thickness of the retinal ganglion cell layer (RGCL) and global retinal nerve fiber layer thickness (gRNFL) were measured using SPECTRALIS[®] optical coherence tomography (Heidelberg Engineering, Heidelberg, Germany). "Macular grid" was used to study the region of the macula lutea. On the basis of a $30^\circ \times 25^\circ$ volume scan of the macula the macular grid is defined by an elliptical ring (**Figure 1A**): the inner radius was 0.618 mm in

the horizontal axis and the inner radius of the vertical axis was 0.531 mm. Outer radius of the elliptical ring was 1.857 mm horizontally and 1.590 mm vertically. The elliptical ring was divided into 6 sectors with angles of 60°. These 6 sectors of the macula grid corresponded to the superior (S), inferior (I), temporal-superior (TS), temporal-inferior (TI), nasal-superior (NS), and nasal-inferior (NI) macular region. Macular grid is normalized to the axis between the center of Bruch's membrane opening of the disc and the foveola (Anatomic Positioning System, APS).

Thickness of RGCL was measured (μm) by Spectralis II (Heidelberg, Germany). Sectorial and global mean ("global value "GV") were presented, respectively. The sectors of the macular grid in so-called deviation maps were color-coded according to percentiles (**Figure 1B**): A sector is marked with green if thickness of the RGCL in this sector is $>5\%$ percentile of a healthy reference population (16). If a sector is colored yellow, the value of the average RGCL thickness $< 5\%$ percentile, yet $> 1\%$ percentile of the reference database. A red colored sector represented data which were $< 1\%$ percentile. The

TABLE 3 | Global and sectorial RGCL thickness (median, quartiles; μm) of all subgroups (OHT, pre-OAG, NTG, POAG, SOAG, controls); GV, global value; TS, temporal superior; S, superior; NS, nasal superior; NI, nasal inferior; I, inferior; TI, temporal inferior; p-values (p) for comparison of each subgroup with controls for quantitative RGCL thickness (μm , Bonferroni-corrected).

	OHT	Pre-OAG	POAG
GV	51.5 (47.0–55.0) $p > 0.05$	45.0 (37.0–49.0) $p < 0.05$	35.0 (27.8–40.0) $p < 0.001$
TS	48.5 (43.6–52.0) $p > 0.05$	38.0 (29.0–47.0) $p < 0.05$	29.0 (21.0–41.0) $p < 0.001$
S	53.0 (48.8–56.3) $p > 0.05$	45.0 (35.0–51.0) $p < 0.05$	39.5 (30.0–45.3) $p < 0.001$
NS	52.0 (48.0–56.0) $p > 0.05$	47.0 (41.0–52.0) $p < 0.05$	39.5 (30.8–47.5) $p < 0.001$
NI	52.5 (48.8–56.0) $p > 0.05$	48.0 (41.0–52.0) $p > 0.05$	41.0 (32.8–44.8) $p < 0.001$
I	52.5 (49.0–54.0) $p > 0.05$	48.0 (40.0–51.0) $p < 0.05$	32.5 (24.8–42.3) $p < 0.001$
TI	51.5 (47.0–53.0) $p > 0.05$	45.0 (35.0–50.0) $p < 0.05$	27.0 (19.8–40.0) $p < 0.001$
	NTG	SOAG	Controls
GV	38.0 (29.0–42.0) $p < 0.001$	29.0 (24.3–38.3) $p < 0.001$	52.0 (48.3–53.0) 47.5 (44.0–50.0)
TS	31.0 (24.0–39.0) $p < 0.001$	23.5 (20.3–31.8) $p < 0.001$	53.0 (48.8–54.8) 53.5 (48.5–55.0)
S	40.0 (29.0–50.0) $p < 0.001$	29.0 (25.3–37.3) $p < 0.001$	53.0 (49.3–55.8) 52.0 (51.0–54.8)
NS	43.0 (35.0–52.0) $p < 0.001$	35.5 (26.3–44.0) $p < 0.001$	51.0 (47.5–52.8)
NI	45.0 (31.0–50.0) $p < 0.01$	33.0 (23.0–44.8) $p < 0.001$	
I	34.0 (24.0–45.0) $p < 0.001$	28.5 (24.0–38.8) $p < 0.001$	
TI	24.0 (18.0–40.0) $p < 0.001$	23.5 (18.8–34.3) $p < 0.001$	

SPECTRALIS[®] retinal thickness reference database is based on data of 255 eyes of 255 healthy patients of European origin. Data in this database were corrected due for age and the distance between fovea and BMO center using a multiple linear regression model. The study was done in accordance with the Helsinki Declaration and was approved by the ethics committee of the University of Erlangen-Nürnberg.

Extended Macular Grid

The SPECTRALIS[®] software measures a much larger retinal section than the central macular grid covers for RGCL analysis and these thickness deviation maps are also color-coded. Yet, only qualitative, no quantitative data of RGCL are available for this “extended” region.

An enlarged elliptical ring was added to the pre-existing macular grid (extended macular grid, **Figure 1C**): 3.714 mm horizontally and 3.18 mm vertically (i.e., doubled outer radii of the original macular grid, respectively). This resulted in 6 new outer sectors (o). The outer sectors were called outer superior (oS), outer inferior (oI), outer temporal-superior (oTS), outer temporal-inferior (oTI), outer nasal-superior (oNS), and outer nasal-inferior (oNI). Combining each original macular grid sector with its corresponding outer sector (for example

eS = S + oS), extended sectors were created: extended superior (eS), extended inferior (eI), extended temporal-superior (eTS), extended temporal-inferior (eTI), extended nasal-superior (eNS), and extended nasal-inferior (eNI) sector.

Statistical Analysis

Statistical analysis was done using the SPSS Version 24.0. A non-parametric test (Mann-Whitney-U-Test) was used. All results were corrected according to Bonferroni considering multiple testing. A quantitative and qualitative analysis of the RGCL thickness were done. A self-developed point score was designed for qualitative analysis (see below). To compare statistical power of different ROCs, sensitivity, and specificity were calculated. When calculating sensitivity and specificity, cut-off was selected as the point where Youden index had its maximum (i.e., optimum sensitivity and specificity) (17).

Quantitative Analysis

Quantitative analysis measured the absolute RGCL thickness [μm] for each sector, respectively. In addition, mean of all sectors was calculated (i.e., global value; GV). Receiver Operating Characteristic (ROC) curves were performed considering each sector individually and GV.

Qualitative Analysis

For the qualitative analysis of the RGCL a point scoring was allocated to each sector of the macula grid (**Figure 1B**):

- red: 3 points
- yellow: 2 points
- green: 1 point

This point scoring of all sectors was summed up (i.e., qualitative total value; QTV). ROC curves were done for each sector of the macula grid and QTV.

Qualitative Analysis of the Extended Macular Grid

For the qualitative analysis of the RGCL thickness of the extended macular grid (**Figure 1C**) an additional point scoring was established. The following points were allocated for each of the 12 sectors (there had to be a cluster of at least 3 pixels to be counted valid):

- Only green (complete sector): 0 points
- Only yellow and $\leq 50\%$ of the area in one sector: 1 point
- Only yellow and $> 50\%$ of the area in one sector: 2 points
- Yellow and red and $\leq 50\%$ of the area in one sector: 3 points
- Yellow and red and $> 50\%$ of the area in one sector: 4 points
- Only red (complete sector): 5 points

The points of an extended sector were obtained by summing up the points from the outer sector with its corresponding sector from the original macular grid (for example points eS = points S + points oS). This point scoring of all extended sectors was summed up (i.e., extended qualitative total value; eQTV). ROC curves were done for each extended sector of the extended macula grid and eQTV.

TABLE 4 | AUC of ROC analysis of quantitative RGCL thickness for each subgroup (OHT, pre-OAG, NTG, POAG, SOAG vs. controls, respectively): global (GV, global value) and sectorial (TS, temporal superior; S, superior; NS, nasal superior; NI, nasal inferior; I, inferior; TI, temporal inferior).

		TS	S	NS	NI	I	TI	GV
OHT-controls	AUC	0.561	0.525	0.534	0.513	0.523	0.512	0.526
Pre-OAG-controls	AUC	0.748	0.763	0.742	0.708	0.78	0.795	0.772
NTG-controls	AUC	0.88	0.9	0.859	0.845	0.883	0.882	0.916
POAG-controls	AUC	0.903	0.926	0.886	0.884	0.937	0.945	0.942
SOAG-controls	AUC	0.977	0.959	0.936	0.918	0.965	0.947	0.965

RESULTS

Quantitative Analysis

Median and quartiles of RGCL thickness for GV and each sector can be seen in **Table 3**. In addition, **Table 3** shows *p*-values for all comparison groups. GV differed significantly between pre-OAG, NTG, POAG, SOAG, and controls (*p* < 0.05), respectively. Yet, no significant difference was observed between OHT and controls (*p* > 0.05).

ROC analysis of quantitative RGCL thickness is shown in **Table 4**. GV yielded highest AUCs for SOAG, POAG, and NTG vs. controls, respectively (>0.9). Sectorial analysis for these subgroups ranged between 0.882 and 0.977. AUCs of OHT vs. controls showed values between 0.5 and 0.6.

Qualitative Analysis

Median and quartiles of RGCL thickness score can be found in **Table 5**. *P*-values for all comparison groups are shown in **Table 5**. QTV of RGCL thickness score differed significantly between pre-OAG, NTG, POAG, SOAG, and controls (*p* < 0.05), respectively. Yet, not significant difference was observed between OHT and controls (*p* > 0.05).

ROC analysis of qualitative RGCL thickness score is shown in **Table 6**. QTV showed highest AUC for SOAG, POAG and NTG vs. controls, respectively (>0.9).

Comparison Quantitative vs. Qualitative Analysis

Comparing ROC curves of QTV and GV yielded similar AUC for each subgroup analysis (**Figure 2**). Mean difference between AUC of GV and QTV (Δ_{GV-QTV}) was 0.02 ± 0.016 for the total cohort. Subgroup analysis showed a Δ_{GV-QTV} of 0.007 (OHT vs. control), 0.043 (pre-OAG vs. controls), 0.008 (NTG vs. controls), 0.028 (POAG vs. controls), and 0.035 (SOAG vs. controls). Δ_{GV-QTV} plotted against their corresponding average can be seen in **Figure 3** for each subgroup, respectively.

Qualitative Analysis of Extended Macular Grid

Median and quartiles of extended RGCL thickness score is shown in **Table 7**. *P*-values for all comparison groups can be seen in **Table 7**. EQTV differed significantly between pre-OAG, NTG, POAG, SOAG, and controls (*p* < 0.05), respectively. Yet, not significant difference was observed between OHT and controls (*p* > 0.05).

TABLE 5 | Total and sectorial RGCL thickness score (median, quartiles) of all subgroups (OHT, pre-OAG, NTG, POAG, SOAG, controls): QTV, qualitative total value; TS, temporal superior; S, superior; NS, nasal superior; NI, nasal inferior; I, inferior; TI, temporal inferior; *p*-values (*p*) for comparison of each subgroup with controls (Bonferroni-corrected).

	OHT	Pre-OAG	POAG
QTV	0.0 (0.0–0.0) <i>p</i> > 0.05	1.0 (0.0–7.0) <i>p</i> < 0.05	8.0 (4.0–11.0) <i>p</i> < 0.001
TS	0.0 (0.0–0.0) <i>p</i> > 0.05	0.0 (0.0–2.0) <i>p</i> < 0.05	2.0 (0.0–2.0) <i>p</i> < 0.001
S	0.0 (0.0–0.0) <i>p</i> > 0.05	0.0 (0.0–2.0) <i>p</i> < 0.05	1.5 (0.0–2.0) <i>p</i> < 0.001
NS	0.0 (0.0–0.0) <i>p</i> > 0.05	0.0 (0.0–1.0) <i>p</i> > 0.05	1.0 (0.0–2.0) <i>p</i> < 0.001
NI	0.0 (0.0–0.0) <i>p</i> > 0.05	0.0 (0.0–1.0) <i>p</i> > 0.05	1.0 (0.0–2.0) <i>p</i> < 0.001
I	0.0 (0.0–0.0) <i>p</i> > 0.05	0.0 (0.0–1.0) <i>p</i> > 0.05	2.0 (0.0–2.0) <i>p</i> < 0.001
TI	0.0 (0.0–0.0) <i>p</i> > 0.05	0.0 (0.0–2.0) <i>p</i> < 0.05	2.0 (0.8–2.0) <i>p</i> < 0.001
	NTG	SOAG	Controls
QTV	6.0 (3.0–12.0) <0.001	11.5 (6.0–12.0) <i>p</i> < 0.001	(0.0–0.0) (0.0–0.0)
TS	2.0 (0.0–2.0) <i>p</i> < 0.05	2.0 (2.0–2.0) <i>p</i> < 0.001	(0.0–0.0) (0.0–0.0)
S	1.0 (0.0–2.0) >0.05	2.0 (2.0–2.0) <i>p</i> < 0.001	(0.0–0.0) (0.0–0.0)
NS	0.0 (0.0–2.0) >0.05	2.0 (0.0–2.0) <0.01	0.0 (0.0–0.0)
NI	0.0 (0.0–2.0) >0.05	2.0 (0.0–2.0) <0.05	
I	2.0 (0.0–2.0) <0.05	2.0 (1.3–2.0) <i>p</i> < 0.001	
TI	2.0 (1.0–2.0) <0.05	2.0 (1.3–2.0) <i>p</i> < 0.001	

ROC analysis of extended macular grid is shown in **Table 8**. EQTV yielded highest AUCs for SOAG, POAG, and NTG vs. controls, respectively (>0.9). Also, sectorial analysis reached high AUC values (**Table 8**).

Comparison of Quantitative (Macular Grid) Analysis vs. Extended Qualitative Analysis (Using Extended Macular Grid) and Global RNFL

Comparing ROC curves of GV and eQTV it can be noticed that eQTV yielded higher AUCs than GV in the comparison groups

TABLE 6 | AUC of ROC analysis of qualitative RGCL thickness score for each subgroup (OHT, pre-OAG, NTG, POAG, SOAG vs. controls, respectively): total (QTV, qualitative total value) and sectorial (TS, temporal superior; S, superior; NS, nasal superior; NI, nasal inferior; I, inferior; TI, temporal inferior).

		TS	S	NS	NI	I	TI	QTV
OHT-controls	AUC	0.528	0.51	0.538	0.508	0.531	0.519	0.519
Pre-OAG-controls	AUC	0.711	0.683	0.654	0.629	0.616	0.667	0.729
NTG-controls	AUC	0.857	0.747	0.737	0.692	0.832	0.895	0.908
POAG-controls	AUC	0.81	0.832	0.794	0.806	0.826	0.882	0.914
SOAG-controls	AUC	0.932	0.9	0.81	0.799	0.93	0.938	0.93

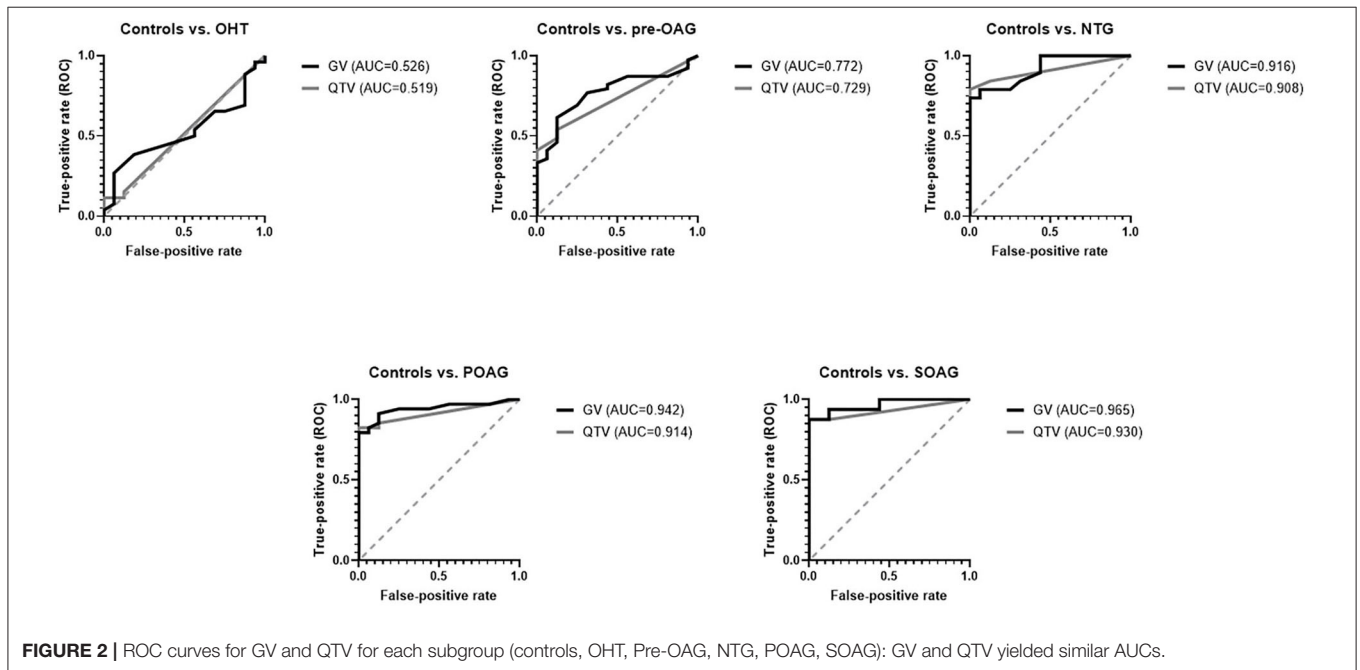


FIGURE 2 | ROC curves for GV and QTV for each subgroup (controls, OHT, Pre-OAG, NTG, POAG, SOAG): GV and QTV yielded similar AUCs.

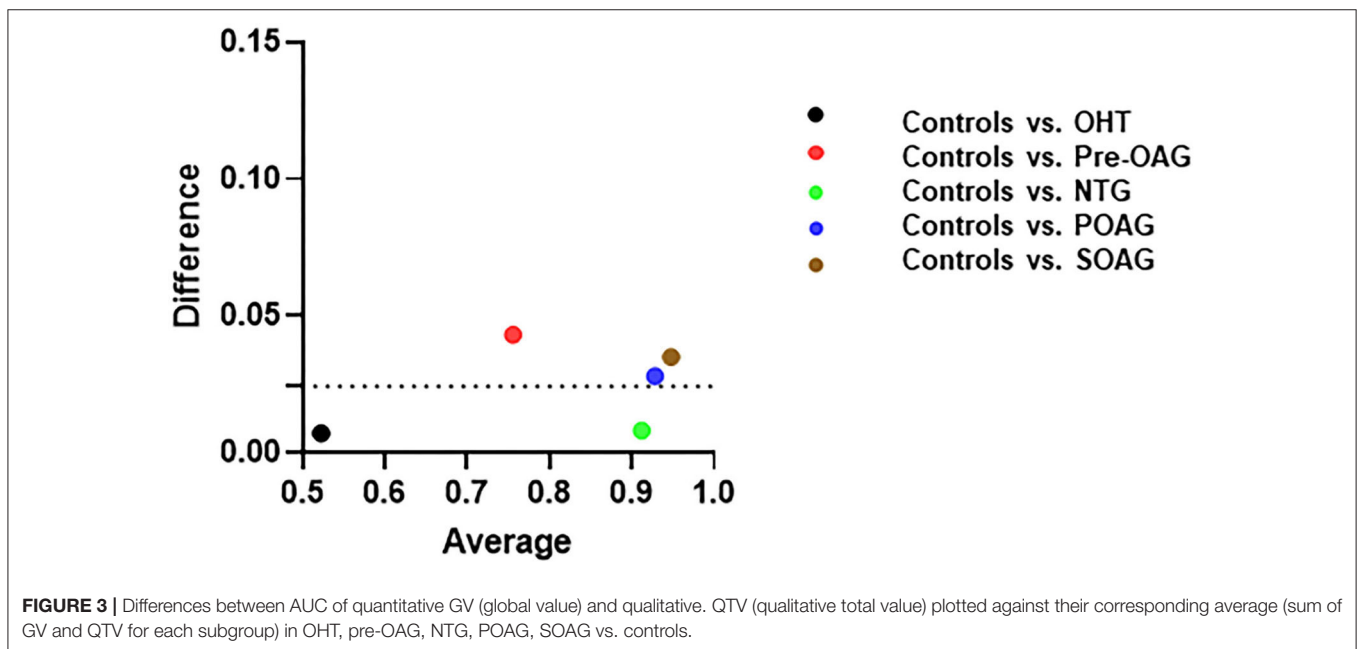


FIGURE 3 | Differences between AUC of quantitative GV (global value) and qualitative. QTV (qualitative total value) plotted against their corresponding average (sum of GV and QTV for each subgroup) in OHT, pre-OAG, NTG, POAG, SOAG vs. controls.

TABLE 7 | Extended QTV (qualitative total value) and extended sector scoring of RGCL thickness (median, quartiles) of all subgroups (OHT, pre-OAG, NTG, POAG, SOAG, controls); eQTV, extended qualitative total value; eTS, extended temporal superior; eS, extended superior; eNS, extended nasal superior; eNI, extended nasal inferior; eI, extended inferior; eTI, extended temporal inferior; p-values (p) for comparison of each subgroup with controls (Bonferroni-corrected).

	OHT	Pre-OAG	POAG
eQTV	5.0 (3.0–12.3) >0.05	20.0 (8.0–42.0) <0.01	40.0 (31.8–46.3) <0.001
eTS	1.0 (0.0–3.0) >0.05	5.0 (1.0–7.0) <0.01	7.0 (4.8–8.0) <0.001
eS	1.0 (0.0–3.0) >0.05	4.0 (1.0–7.0) <0.01	7.5 (4.0–8.0) <0.001
eNS	1.0 (0.0–2.3) >0.05	4.0 (0.0–7.0) >0.05	7.0 (4.0–7.0) <0.001
eNI	0.0 (0.0–3.0) >0.05	2.0 (1.0–7.0) >0.05	7.0 (6.0–7.0) <0.001
eI	0.0 (0.0–1.0) >0.05	3.0 (0.0–7.0) >0.05	7.0 (3.8–8.0) <0.001
eTI	0.0 (0.0–3.0) >0.05	4.0 (0.0–7.0) <0.05	8.0 (6.8–8.0) <0.001
	NTG	SOAG	Controls
eQTV	40.0 (32.0–45.0) <0.001	11.5 (6.0–12.0) <0.001	43.5 (35.5–47.0) 8.0 (7.0–8.0)
eTS	7.0 (4.8–8.0) <0.001	2.0 (2.0–2.0) <0.001	8.5 (7.0–8.0) 7.0 (4.5–8.0)
eS	7.5 (4.0–8.0) <0.001	2.0 (2.0–2.0) <0.001	7.0 (5.3–7.0) 7.0 (5.5–8.0)
eNS	7.0 (4.0–7.0) <0.05	2.0 (0.0–2.0) <0.01	8.0 (7.0–8.0)
eNI	7.0 (6.0–7.0) <0.001	2.0 (0.0–2.0) <0.05	
eI	7.0 (3.8–8.0) <0.001	2.0 (1.3–2.0) <0.001	
eTI	8.0 (6.8–8.0) <0.001	2.0 (1.3–2.0) <0.001	

SOAG, POAG, and NTG vs. controls, respectively (**Figure 4**). At fixed specificity of 100% GV and eQTV had the same sensitivity in SOAG vs. controls; in NTG vs. controls sensitivity of eQTV was even higher (**Table 9**). In the two remaining subgroups (OHT, pre-OAG), the AUCs of eQTV and GV behaved similarly (**Figure 4** and **Table 9**). In SOAG vs. controls, AUC of global RNFL behaved similarly to AUC of eQTV and GV. Sensitivity and specificity in this subgroup were the same for GV, eQTV, and global RNFL (**Table 9**). In POAG vs. controls, AUC of global RNFL was smaller than GV and eQTV. In NTG, pre-OAG, and OHT vs. controls, respectively, global RNFL had the highest AUC (**Table 9**).

DISCUSSION

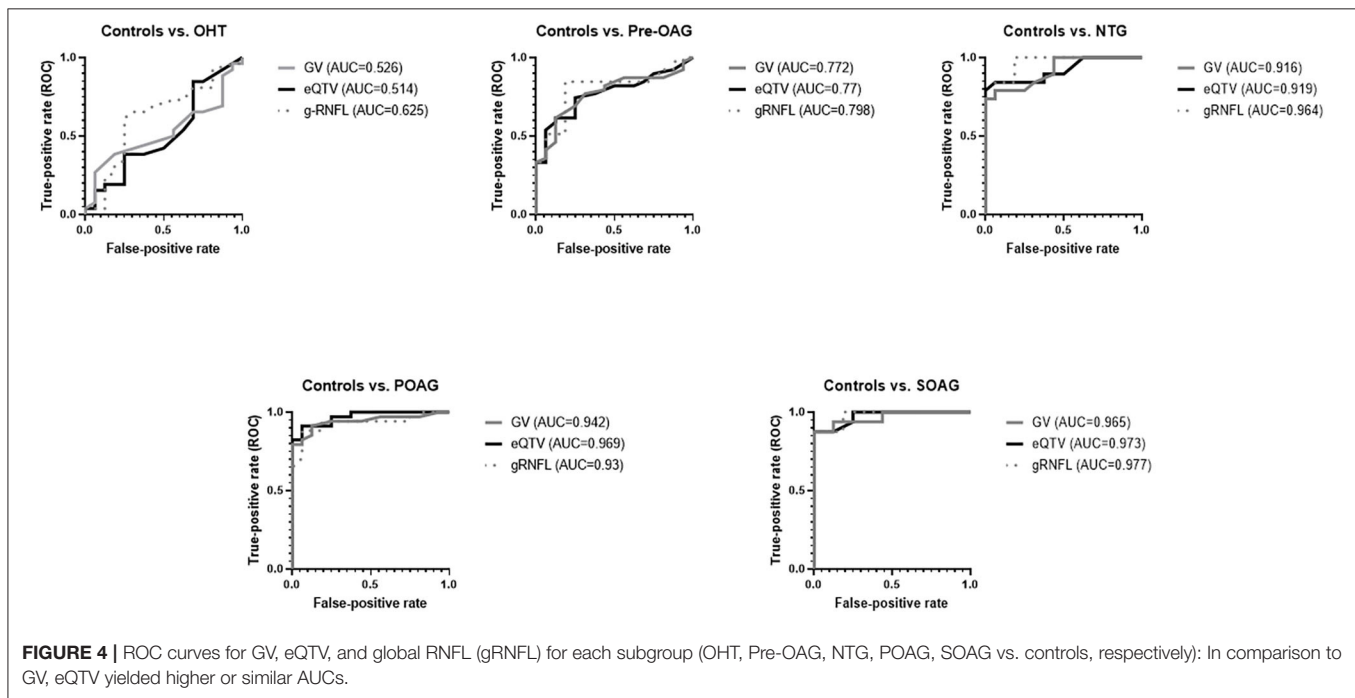
By 2040, the number of patients with glaucoma will have risen to 111.8 million worldwide, visualizing the impact of glaucoma disease (18). Glaucoma is a multifactorial disease with an elevated IOP as most important risk factor, known until now (19). Several studies showed that an increased IOP leads to RGC loss (20–25). One molecular mechanism might be seen in the

presence of mechanosensitive Piezo channels within the GCL (26). Piezo channels enable cells to convert a mechanical force into a molecular signaling by detection of e.g., shear stress. After activation of Piezo channels a non-selective influx of cations into the cell generates membrane depolarization and activation of different signaling pathways (Ca²⁺ dependent) (27). Interestingly, the number of retinal Piezo 2 channels within the RGCL was increased after elevating IOP in an animal model (mice) (26). Morphometric measurements of RGCL seem to be prior compared to functional tests (28). It was shown that macular thickness measured by OCT can be considered as a surrogate indicator of RGC loss (29). Especially, in myopic eyes macular GCC thickness measurement performed better than RNFL (30). The present study showed that even looking at the qualitative analysis of RGCL data, yielded a similar diagnostic impact as quantitative data. This has a very practical impact in everyday clinical work where areas of ganglion cell layer thinning can immediately be noticed by an examiner. In addition, implementation of an enlarged macular grid in RGCL analysis was very well-suited to distinguish healthy from glaucoma subjects. It is notable that purely qualitative analysis of the enlarged macular grid—using a point score—yielded higher or at least similar good AUCs compared to the quantitative analysis of conventional smaller macular grid.

Data from earlier studies showed that there is a significant difference in macular thickness volume between healthy subjects and those with glaucoma. However, the diagnostic power did not approach that of the RNFL (31, 32). The diagnostic power was increased by introduction of macular segmentation algorithms, showing similar diagnostic value to RNFL (33, 34). To the best of our knowledge, the present study is the first one, investigating single macular RGCL thickness with the conventional SPECTRALIS[®] grid and enlarged grid in deviation maps in different types of glaucoma. All recent studies aimed on analysis of the ganglion cell complex (i.e., IPL, GCL, and RNFL) or GCIPL (ganglion cell–inner plexiform layer, i.e., RGCL and IPL) (7, 12, 13). Analyzing average macular GCIPL thickness AUCs of 0.590 (glaucoma suspects vs. controls), 0.668 (early glaucoma vs. controls), and 0.614 (glaucoma suspect and early glaucoma vs. controls) were observed, measured by Cirrus HD-OCT (Carl Zeiss Meditec, Inc., Dublin, CA) (12). AUCs of 0.806 and 0.929 were presented for GCC data, based on measurements with RTVue-100 (Optovue Inc., Fremont, CA) when comparing early glaucoma and advanced glaucoma vs. controls, respectively (35). Next to the differences in measurement of the retinal layers, different grids were used by the two devices: Cirrus HD-OCT measures GCIPL within an elliptical annulus centered on the fovea within an area of 14.13 mm² in six sectors (superotemporal, superior, superonasal, inferonasal, inferior, inferotemporal) and calculates an average value for the whole grid (7, 13). RTVue-100 measures GCC by a square grid of 7 × 7 mm located on the central macula. Quantitative data given by the software include the average thickness and hemifield thickness (superior and inferior) of GCC. Furthermore, the software gives two additional parameters: focal loss volume (FLV) (i.e., average amount of focal GCC loss divided by map area) and global loss volume (GLV) (i.e., sum of all negative

TABLE 8 | AUC of ROC analysis of extended qualitative RGCL thickness score for each subgroup (OHT, pre-OAG, NTG, POAG, SOAG vs. controls, respectively); total (eQTV, extended qualitative total value) and sectorial (eTS, extended temporal superior; eS, extended superior; eNS, extended nasal superior; eNI, extended nasal inferior; eI, extended inferior; eTI, extended temporal inferior).

		eTS	eS	eNS	eNI	eI	eTI	eQTV
OHT-controls	AUC	0.516	0.581	0.594	0.52	0.553	0.519	0.514
Pre-OAG-controls	AUC	0.788	0.765	0.667	0.691	0.685	0.744	0.77
NTG-controls	AUC	0.901	0.929	0.793	0.890	0.908	0.933	0.919
POAG-controls	AUC	0.925	0.910	0.931	0.943	0.938	0.96	0.969
SOAG-controls	AUC	0.949	0.98	0.891	0.924	0.924	0.969	0.973



fractional deviations within the whole area of the map) (36). Especially, data of the inferior hemifield yielded highest AUCs: AUC 0.75 (pre-OAG vs. controls) (37), AUC of 0.815 (pre-OAG vs. controls) (35), AUC of 0.715 (early glaucoma vs. OHT/controls) (38), and AUC of 0.827 (POAG vs. controls). (38) These results are in accordance with the quantitative data of the macular RGCL thickness in the present study. Highest AUCs were observed in sector TI (AUC = 0.795) and sector I (AUC = 0.78) for controls vs. pre-OAG. In the extended grid sector eTS and eQTV yielded the highest AUCs (0.788, 0.77) for this subgroup. Contrary, the superior hemifield of GCC was observed to be the best for diagnosing glaucoma in eyes with pre-POAG (AUC 0.84 and 0.76) in only one previous study (39).

As an increased IOP induced RGC loss (20–25), devices, investigating thickness of single RGC layer, might improve the diagnostic value of GCC/GCIPL. SPECTRALIS[®] offers the possibility of analysis of single GCL layer in a defined macular region with different grids. For one special grid an automatic

deviation map is generated for each single measurement enabling simultaneously quantitative and qualitative (color-coded) analysis. This macular grid is defined by an elliptic ring consisting of six sectors [superior (S), inferior (I), temporal-superior (TS), temporal-inferior (TI), nasal-superior (NS), and nasal-inferior (NI)]. To best of our knowledge, up to know there is no study available on GCL data of the deviation map and only one study on GCL analysis in eyes with NTG measured by SPECTRALIS[®] (40). An enhanced stratification of the retina might offer an improved and even finer analysis of pathological alterations. Thus, affections of RGCL might be observed in even earlier stages of disease. Data of the only recent study showed that macular RGCL was significantly thinner in patients with NTG compared to healthy controls (1, 3, 6 mm ETDRS grid). The highest AUC value was reached in superior outer macula sector (0.863), confirming data of the present study (0.9). It is notable that outer sectors yielded generally higher AUC values (0.863, 0.837) than inner sectors (0.747, 0.747) in a previous (1, 3, 6 mm ETDRS grid) (40)

TABLE 9 | Sensitivity, specificity and AUCs of ROC for GV [μm], QTV, eQTV, and global RNFL [μm] for OHT, pre-OAG, NTG, POAG, and SOAG vs. controls, respectively.

		Cut-off	Sensitivity %	Specificity %	AUC
OHT vs. controls	GV	54.5	26.9	93.8	0.526
	QTV	2.5	11.5	100	0.519
	eQTV	2.5	84.6	31.3	0.514
	global RNFL	93.5	61.5	75.0	0.625
Pre-OAG vs. controls	GV	47.5	61.5	87.5	0.772
	QTV	0.5	53.8	87.5	0.729
	eQTV	8.5	74.4	75.0	0.77
	global RNFL	86.5	84.6	81.3	0.798
NTG vs. controls	GV	40.5	73.7	100	0.916
	QTV	2.5	78.9	100	0.908
	eQTV	31	78.9	100	0.919
	global RNFL	86.5	100	81.3	0.964
POAG vs. controls	GV	40.5	79.4	100	0.942
	QTV	2.5	82.4	100	0.914
	eQTV	18	91.2	93.8	0.969
	global RNFL	76.5	88.2	93.8	0.930
SOAG vs. controls	GV	40.5	87.5	100	0.965
	QTV	3.5	87.5	100	0.93
	eQTV	31	87.5	100	0.973
	global RNFL	69.5	87.5	100	0.977

The cut-off was selected as the point where Youden index had its maximum in each ROC curve (i.e. optimum for sensitivity and specificity).

and present study [macular grid; eTI (0.933), eQTV (0.919)]. In addition, the outer superior sector of the ETDRS grid yielded the best AUC for differentiating between eyes with primary open-angle glaucoma and controls (AUC = 0.840) (41). Even analysis of macula GCC thickness showed that enlarged grids improved discrimination between glaucoma subjects and controls compared to a smaller standard grid (11). Using the enlarged macular grid, qualitative analysis yielded highest AUCs for sector TI (0.96) and eQTV (0.969; POAG vs. controls) and for sector eS (0.98) and eQTV (0.973, SOAG vs. controls) for the present study cohort. This may reflect the observation that in high-tension open-angle glaucoma loss of ganglion cells are found more to the peripheral macula. In normal-tension glaucoma GCL and visual field defects tend to be more located in the perifoveolar area. This observation may be reflected by our finding that GV and eQTV yielded similar AUC values (0.916 vs. 0.919, respectively).

The study is not without limitations. Patients' cohort is rather small, yet all patients were well-known study participants of the Erlangen Glaucoma Registry and had a follow-up for several years. So, there was no doubt about their clinical classification of disease severity. Furthermore, the extended grid could only be evaluated semi-quantitatively and analysis could not be analyzed in comparison to absolute values. Nevertheless, we used the color-coded information to show, that there is much more information in the whole macular scan than in software's central, standard grid. Color-coded information has the great advantage for clinical examiners to detect deviation of topographic RGCL thickness measurements from normal in

a glance. We could show that this clinically comprehensive, qualitative approach showed similar discrimination in the central grid as the absolute, quantitative values. Thirdly, in the analysis the total area of the deviation map was not considered. Probably there would have been even more information on RGCL thickness deviation from normal, in doing so, but we tried to standardize the area of investigation using an extended circle with a fixed prolongation of the software's central, standard grid.

CONCLUSION

The results indicate that analysis of RGCL thickness could represent a valuable parameter in glaucoma diagnosis, being comparable to analysis of RNFL. Quantitative analysis showed that AUCs of 0.772 to even 0.965 can be obtained. Analysis of an extended macular region might improve its diagnostic impact. Furthermore, qualitative analysis using the standard macular grid yielded even similar diagnostic impacts compared to quantitative analysis. Clinical practitioners might use this quantitative analysis in their clinical all-day life.

DATA AVAILABILITY STATEMENT

The original contributions presented in the study are included in the article/supplementary material, further inquiries can be directed to the corresponding authors.

ETHICS STATEMENT

The studies involving human participants were reviewed and approved by the study was approved by the ethics committee of the University of Erlangen-Nürnberg. The patients/participants provided their written informed consent to participate in this study.

AUTHOR CONTRIBUTIONS

PL: data analysis and writing of the draft of the manuscript. BH: supervision, revision of the manuscript, and clinical study. RL: clinical study. CM: supervision, revision of the manuscript, and clinical study.

REFERENCES

- Flaxman SR, Bourne RRA, Resnikoff S, Ackland P, Braithwaite T, Cicinelli MV, et al. Global causes of blindness and distance vision impairment 1990–2020: a systematic review and meta-analysis. *Lancet Glob Health*. (2017) 5:e1221–34. doi: 10.1016/S2214-109X(17)30393-5
- Wang W, He M, Li Z, Huang W. Epidemiological variations and trends in health burden of glaucoma worldwide. *Acta Ophthalmol*. (2019) 97:e349–55. doi: 10.1111/aos.14044
- Jutley G, Luk SM, Dehabadi MH, Cordeiro MF. Management of glaucoma as a neurodegenerative disease. *Neurodegener Dis Manag*. (2017) 7:157–72. doi: 10.2217/nmt-2017-0004
- Jonas JB, Aung T, Bourne RR, Bron AM, Ritch R, Panda-Jonas S. Glaucoma. *Lancet*. (2017) 390:2183–93. doi: 10.1016/S0140-6736(17)31469-1
- Bertaud S, Aragno V, Baudouin C, Labbe A. [Primary open-angle glaucoma]. *Rev Med Interne*. (2019) 40:445–52. doi: 10.1016/j.revmed.2018.12.001
- Joachim SC, Jehle T, Boehm N, Gramlich OW, Lagreze WA, Pfeiffer N, et al. Effect of ischemia duration on autoantibody response in rats undergoing retinal ischemia-reperfusion. *Ophthalmic Res*. (2012) 48:67–74. doi: 10.1159/000335965
- Scuderi G, Fragiotta S, Scuderi L, Iodice CM, Perdicchi A. Ganglion cell complex analysis in glaucoma patients: what can it tell us? *Eye Brain*. (2020) 12:33–44. doi: 10.2147/EB.S226319
- Iorga RE, Moraru A, Ozturk MR, Costin D. The role of optical coherence tomography in optic neuropathies. *Rom J Ophthalmol*. (2018) 62:3–14. doi: 10.22336/rjo.2018.2
- Zhang X, Dastiridou A, Francis BA, Tan O, Varma R, Greenfield DS, et al. Comparison of glaucoma progression detection by optical coherence tomography and visual field. *Am J Ophthalmol*. (2017) 184:63–74. doi: 10.1016/j.ajo.2017.09.020
- Ng DS, Gupta P, Tham YC, Peck CF, Wong TY, Ikram MK, et al. Repeatability of perimacular ganglion cell complex analysis with spectral-domain optical coherence tomography. *J Ophthalmol*. (2015) 2015:605940. doi: 10.1155/2015/605940
- Kim HJ, Park KH, Kim YK, Jeoung JW. Evaluation of layer-by-layer segmented ganglion cell complex thickness for detecting early glaucoma according to different macular grids. *J Glaucoma*. (2017) 26:712–7. doi: 10.1097/IJG.0000000000000709
- Aquino LG, Aquino NM. Evaluation of macular ganglion cell layer thickness vs peripapillary retinal nerve fiber layer thickness for glaucoma detection using spectral-domain optical coherence tomography in a tertiary Philippine hospital. *J Curr Glaucoma Pract*. (2020) 14:50–6. doi: 10.5005/jp-journals-10078-1278
- Hwang YH, Jeong YC, Kim HK, Sohn YH. Macular ganglion cell analysis for early detection of glaucoma. *Ophthalmology*. (2014) 121:1508–15. doi: 10.1016/j.ophtha.2014.02.019
- Alshareef RA, Dumpala S, Rapole S, Januwada M, Goud A, Peguda HK, et al. Prevalence and distribution of segmentation errors in macular ganglion cell analysis of healthy eyes using cirrus HD-OCT. *PLoS ONE*. (2016) 11:e0155319. doi: 10.1371/journal.pone.0155319
- Jonas JB, Gusek GC, Naumann GO. Optic disc morphometry in chronic primary open-angle glaucoma. II. Correlation of the intrapapillary morphometric data to visual field indices. *Graefes Arch Clin Exp Ophthalmol*. (1988) 226:531–8. doi: 10.1007/BF02169200
- Chauhan BC, Danthurebandara VM, Sharpe GP, Demirel S, Girkin CA, Mardin CY, et al. Bruch's membrane opening minimum rim width and retinal nerve fiber layer thickness in a normal white population: a multicenter study. *Ophthalmology*. (2015) 122:1786–94. doi: 10.1016/j.ophtha.2015.06.001
- Carter JV, Pan J, Rai SN, Galandiuk S. ROC-ing along: evaluation and interpretation of receiver operating characteristic curves. *Surgery*. (2016) 159:1638–45. doi: 10.1016/j.surg.2015.12.029
- Tham YC, Li X, Wong TY, Quigley HA, Aung T, Cheng CY. Global prevalence of glaucoma and projections of glaucoma burden through 2040: a systematic review and meta-analysis. *Ophthalmology*. (2014) 121:2081–90. doi: 10.1016/j.ophtha.2014.05.013
- Quigley HA, Broman AT. The number of people with glaucoma worldwide in 2010 and 2020. *Br J Ophthalmol*. (2006) 90:262–7. doi: 10.1136/bjo.2005.081224
- Chen H, Wei X, Cho KS, Chen G, Sappington R, Calkins DJ, et al. Optic neuropathy due to microbead-induced elevated intraocular pressure in the mouse. *Invest Ophthalmol Vis Sci*. (2011) 52:36–44. doi: 10.1167/iovs.09-5115
- Wei X, Yu Z, Cho KS, Chen H, Malik MT, Chen X, et al. Neuroglobin is an endogenous neuroprotectant for retinal ganglion cells against glaucomatous damage. *Am J Pathol*. (2011) 179:2788–97. doi: 10.1016/j.ajpath.2011.08.015
- Aptel F, Bron AM, Lachkar Y, Schweitzer C. Change in visual field progression following treatment escalation in primary open-angle glaucoma. *J Glaucoma*. (2017) 26:875–80. doi: 10.1097/IJG.0000000000000748
- Samsel PA, Kisiswa L, Erichsen JT, Cross SD, Morgan JE. A novel method for the induction of experimental glaucoma using magnetic microspheres. *Invest Ophthalmol Vis Sci*. (2011) 52:1671–5. doi: 10.1167/iovs.09-3921
- Urcola JH, Hernandez M, Vecino E. Three experimental glaucoma models in rats: comparison of the effects of intraocular pressure elevation on retinal ganglion cell size and death. *Exp Eye Res*. (2006) 83:429–37. doi: 10.1016/j.exer.2006.01.025
- Biswas S, Wan KH. Review of rodent hypertensive glaucoma models. *Acta Ophthalmol*. (2019) 97:e331–40. doi: 10.1111/aos.13983
- Morozumi W, Inagaki S, Iwata Y, Nakamura S, Hara H, Shimazawa M. Piezo channel plays a part in retinal ganglion cell damage. *Exp Eye Res*. (2020) 191:107900. doi: 10.1016/j.exer.2019.107900
- Parpaite T, Coste B. Piezo channels. *Curr Biol*. (2017) 27:R250–2. doi: 10.1016/j.cub.2017.01.048
- Kerrigan-Baumrind LA, Quigley HA, Pease ME, Kerrigan DF, Mitchell RS. Number of ganglion cells in glaucoma eyes compared with threshold visual field tests in the same persons. *Invest Ophthalmol Vis Sci*. (2000) 41:741–8.
- Greenfield DS, Bagga H, Knighton RW. Macular thickness changes in glaucomatous optic neuropathy detected using optical

FUNDING

The Erlangen Glaucoma Registry was funded by the German Research Society (DFG) from 1991 to 2009, NCT00494923; no specific funding was received for the present study.

ACKNOWLEDGMENTS

The present work was performed in fulfillment of the requirements for obtaining the degree Dr. med. for PL. The Department of Ophthalmology is part of the University of Erlangen-Nürnberg, Friedrich-Alexander-Universität Erlangen-Nürnberg (FAU), Germany.

- coherence tomography. *Arch Ophthalmol.* (2003) 121:41–6. doi: 10.1001/archophth.121.1.41
30. Wang WW, Wang HZ, Liu JR, Zhang XF, Li M, Huo YJ, et al. Diagnostic ability of ganglion cell complex thickness to detect glaucoma in high myopia eyes by Fourier domain optical coherence tomography. *Int J Ophthalmol.* (2018) 11:791–6. doi: 10.18240/ijo.2018.05.12
 31. Lederer DE, Schuman JS, Hertzmark E, Heltzer J, Velazques LJ, Fujimoto JG, et al. Analysis of macular volume in normal and glaucomatous eyes using optical coherence tomography. *Am J Ophthalmol.* (2003) 135:838–43. doi: 10.1016/S0002-9394(02)02277-8
 32. Ojima T, Tanabe T, Hangai M, Yu S, Morishita S, Yoshimura N. Measurement of retinal nerve fiber layer thickness and macular volume for glaucoma detection using optical coherence tomography. *Jpn J Ophthalmol.* (2007) 51:197–203. doi: 10.1007/s10384-006-0433-y
 33. Tan O, Li G, Lu AT, Varma R, Huang D, Advanced Imaging for Glaucoma Study G. Mapping of macular substructures with optical coherence tomography for glaucoma diagnosis. *Ophthalmology.* (2008) 115:949–56. doi: 10.1016/j.ophtha.2007.08.011
 34. Tan O, Chopra V, Lu AT, Schuman JS, Ishikawa H, Wollstein G, et al. Detection of macular ganglion cell loss in glaucoma by Fourier-domain optical coherence tomography. *Ophthalmology.* (2009) 116:2305–14.e1-2. doi: 10.1016/j.ophtha.2009.05.025
 35. Arintawati P, Sone T, Akita T, Tanaka J, Kiuchi Y. The applicability of ganglion cell complex parameters determined from SD-OCT images to detect glaucomatous eyes. *J Glaucoma.* (2013) 22:713–8. doi: 10.1097/IJG.0b013e318259b2e1
 36. Kim NR, Lee ES, Seong GJ, Kim JH, An HG, Kim CY. Structure-function relationship and diagnostic value of macular ganglion cell complex measurement using Fourier-domain OCT in glaucoma. *Invest Ophthalmol Vis Sci.* (2010) 51:4646–51. doi: 10.1167/iovs.09-5053
 37. Rao HL, Addepalli UK, Chaudhary S, Kumbar T, Senthil S, Choudhari NS, et al. Ability of different scanning protocols of spectral domain optical coherence tomography to diagnose preperimetric glaucoma. *Invest Ophthalmol Vis Sci.* (2013) 54:7252–7. doi: 10.1167/iovs.13-12731
 38. Barua N, Sitaraman C, Goel S, Chakraborti C, Mukherjee S, Parashar H. Comparison of diagnostic capability of macular ganglion cell complex and retinal nerve fiber layer among primary open angle glaucoma, ocular hypertension, and normal population using Fourier-domain optical coherence tomography and determining their functional correlation in Indian population. *Indian J Ophthalmol.* (2016) 64:296–302. doi: 10.4103/0301-4738.182941
 39. Na JH, Lee K, Lee JR, Baek S, Yoo SJ, Kook MS. Detection of macular ganglion cell loss in preperimetric glaucoma patients with localized retinal nerve fibre defects by spectral-domain optical coherence tomography. *Clin Exp Ophthalmol.* (2013) 41:870–80. doi: 10.1111/ceo.12142
 40. Lin JB, Lin PW, Lai IC, Tsai JC. Segmental inner macular layer analysis with spectral-domain optical coherence tomography for early detection of normal tension glaucoma. *PLoS ONE.* (2019) 14:e0210215. doi: 10.1371/journal.pone.0210215
 41. Morales-Fernandez L, Jimenez-Santos M, Martinez-de-la-Casa JM, Sanchez-Jean R, Nieves M, Saenz-Frances F, et al. Diagnostic capacity of SD-OCT segmented ganglion cell complex versus retinal nerve fiber layer analysis for congenital glaucoma. *Eye.* (2018) 32:1338–44. doi: 10.1038/s41433-018-0077-4
- Conflict of Interest:** The authors declare that the research was conducted in the absence of any commercial or financial relationships that could be construed as a potential conflict of interest.
- Copyright © 2021 Lehmann, Hohberger, Lämmer and Mardin. This is an open-access article distributed under the terms of the Creative Commons Attribution License (CC BY). The use, distribution or reproduction in other forums is permitted, provided the original author(s) and the copyright owner(s) are credited and that the original publication in this journal is cited, in accordance with accepted academic practice. No use, distribution or reproduction is permitted which does not comply with these terms.